ELSEVIER

Seminars in
ULTRASOUND
CT and MRI

Advanced Imaging in Musculoskeletal Oncology: Moving Away From RECIST and Embracing Advanced Bone and Soft Tissue Tumor Imaging (ABASTI) - Part I - Tumor Response Criteria and Established Functional Imaging Techniques

Raul Fernando Valenzuela, MD, Vikas Kundra, MD, John E. Madewell, MD, and Colleen M. Costelloe, MD

According to the Revised Response Evaluation Criteria in Solid Tumors (RECIST) 1.1, the majority of bone metastases are considered to be nonmeasurable disease. Traditional response criteria rely on physical measurements. New criteria would be valuable if they incorporated newly developed imaging features in order to provide a more comprehensive assessment of oncological status. Advanced magnetic resonance imaging (MRI) sequences such as diffusion-weighted imaging (DWI) and perfusion-weighted imaging (PWI) with dynamic contrast-enhanced (DCE) perfusion imaging are reviewed in the context of the initial and post-therapeutic assessment of musculoskeletal tumors. Particular attention is directed to the pseudoprogression phenomenon in which a successfully treated tumor enlarges from the pretherapeutic baseline, followed by regression without a change in therapy.
Semin Ultrasound CT MRI 42:201-214 Published by Elsevier Inc.

Introduction

This two-part review article presents a current overview of the imaging armamentarium available to the radiologist for the assessment of bone and soft tissue tumors. Part I focuses on RECIST and non-RECIST response criteria. Non-RECIST criteria, such as the MD Anderson Criteria for bone metastases, provide methods for assessing tumor treatment response that go beyond the traditional size and morphologic imaging analysis. Different forms of pseudoprogression, a phenomenon in which a successfully treated tumor can enlarge following chemotherapy, radiation or targeted therapy are also reviewed. Functional MRI can complement morphological imaging, improving tissue characterization, and the staging of bone and soft-tissue tumors. Functional imaging with a focus on the role of diffusion-weighted imaging (DWI) and perfusion-weighted imaging (PWI) are also presented in Part I.

Part II reviews novel techniques and their uses in musculoskeletal oncologic imaging with focus on treatment response evaluation and tumor diagnosis. Techniques such as susceptibility-weighted imaging (SWI), Dixon imaging, whole-body MRI, dual-energy CT (DECT), and ultrasound elastography are discussed. Dixon/chemical-shift MRI offers superior discrimination of marrow infiltrating neoplasms from benign red marrow and because DWI is capable of demonstrating tumor cellularity, thereby helping to distinguish benign and malignant tumors as well as assessing treatment response. PWI and particularly dynamic contrast-enhanced (DCE) perfusion with dynamic gadolinium injection and enhancement time-intensity curve analysis and tumor kinetics assessment,

The University of Texas MD Anderson Cancer Center, Department of Musculoskeletal Imaging, Houston, Texas.
Address reprint requests to Raul Valenzuela, MD, University of Texas MD Anderson Cancer Center, 1515 Holcombe Blvd, Unit 1475, Houston, Texas, 77030. E-mail: rfvalenzuela@mdanderson.org

https://doi.org/10.1053/j.sult.2020.08.012
0887-2171/Published by Elsevier Inc.

has proven useful in evaluating treatment response. This technique is particularly useful when response underestimation may occur with the use of size-based traditional evaluation.[1] Perfusion MRI and diffusion/apparent diffusion coefficient (ADC) mapping can help in the early identification of good responders to chemotherapy. All available functional MRI techniques have limitations that are in part due to overlap of characteristics between benign and malignant histologies. Perfusion MRI, diffusion MRI, and Dixon imaging with in-phase/opposed-phase MRI can be incorporated in routine imaging protocols, increasing diagnostic accuracy for the initial and post-therapeutic assessment of musculoskeletal tumors.

Treatment Response

Tumor Response Criteria

The Revised Response Evaluation Criteria in Solid Tumors (RECIST), version 1.1, are based primarily on the physical measurement of lesions.[2] It is significant to musculoskeletal (MSK) oncologic practice that all bone metastases without a soft-tissue component measuring at least 1 cm in size are considered unmeasurable disease by RECIST 1.1. Examples of other lesions that are considered unmeasurable, affecting many imaging specialties, include ascites, pleural effusion, lymphangitic spread of tumor, leptomeningeal disease, and inflammatory breast cancer.

Advanced functional imaging tools such as PET/CT and dynamic contrast-enhanced MRI (DCE-MRI) have attracted attention as promising methods for tumor response assessment.[3] Because of the complexity of today's oncologic therapies, it would be helpful for future response criteria to include a combination of clinical data, biochemical biomarkers, and tumor-imaging features/imaging biomarkers to provide a more comprehensive view of the neoplastic process. As stated by Schuetze et al, "The RECIST and the World Health Organization (WHO) criteria for evaluation of response in solid tumors need to be modernized. Also, there is a current need for prospective trials to compare new response criteria with established endpoints and to validate imaging-based response rates as surrogate endpoints for clinical trials of new agents for sarcoma and other solid tumors."[4]

Other Imaging Response Criteria Systems in Oncologic Imaging

An example of established disease-specific imaging biomarkers and evaluation systems that do not follow traditional RECIST criteria is the Choi Criteria for treatment response evaluation of gastrointestinal stromal tumors (GIST).[5] The use of tyrosine kinase inhibitors (TKIs) does not necessarily cause a decrease in the size of these tumors. Nevertheless, a reduction in the largest transaxial diameter of 10% or more and a decrease in tumor density by 15% correlates well with good response on FDG-PET and corresponds with positive response (PR). Other examples include the European Association for the Study of the Liver (EASL) guidelines for treatment response evaluation of hepatocellular carcinoma; the modified RECIST assessment for evaluation of hepatocellular carcinoma response to molecular-targeted, or locoregional therapies;[6-8] revised International Workshop Criteria for Lymphoma;[9] and the Criteria for Evaluation of Metastatic Renal Cell Carcinoma Response to Targeted Therapies. Because most metastatic renal cell carcinomas (RCC) are clear cell and hypervascular with high susceptibility to antiangiogenic therapies, optimal response assessment would benefit from volumetric attenuation calculations that require software tools not equally available across institutions.[10,11] The Response Assessment Criteria for High-Grade Gliomas in the Revised Assessment in Neuro-Oncology (RANO) criteria require advanced MRI techniques, such as perfusion, permeability, and diffusion imaging.[12]

An example of non-RECIST criteria regarding MSK imaging is the MD Anderson (MDA) Bone Metastases Response Criteria that include quantitative and qualitative assessments of the behavior of bone metastases.[13-16] As with many other criteria, the responses are classified into the following categories: complete response (CR), characterized by complete sclerotic fill-in of lytic lesions on radiography (XR) or CT, normalization of bone density on XR or CT, normalization of signal intensity on MRI or normalization of tracer uptake on bone scan. When a lesion demonstrates a size reduction of 50% or more in the sum of the perpendicular measurements, it is considered as a PR while progressive disease (PD) is an increase of 25% or more in this sum.[17] In a nonquantitative but practical manner, the MDA response criteria permit the assessment of the density of the lesions on radiography and CT pertaining to evaluation of the treatment effect. A comparison is offered by McDonald et al, who found that the measured degree of local control by the MDA criteria was slightly more significant in the treatment of nonspine bone metastases with stereotactic body radiation therapy (SBRT) when compared with the RECIST 1.1, criteria.[18]

The Challenge of Pseudoprogression in MSK oncology

Pseudoprogression is a phenomenon in which there is an enlargement of a tumor from the pretherapeutic baseline that is followed by radiologic tumor regression without a change in therapy, and without indication of progression on subsequent imaging or pathologic assessment. Different forms of this phenomenon can occur in soft-tissue or bone tumors following different types of treatment, including systemic chemotherapy, radiation, and targeted therapy.[1,19,20] Radiologists must be vigilant to assess for this phenomenon in order to prevent misinterpretation and to ensure the appropriate further evaluation by MRI or PET/CT. The paradoxical increase in tumor size should not be mistaken for progressive disease, and F18 fluorodeoxyglucose (FDG) positron emission tomography (PET) can also help to confirm positive metabolic response (decreased FDG uptake) in these lesions despite the apparent increase in size.

The RECIST 1.1 criteria state that further standardization is needed, including volumetric and functional imaging tools, as part of routine methods for assessing tumor response.[2]

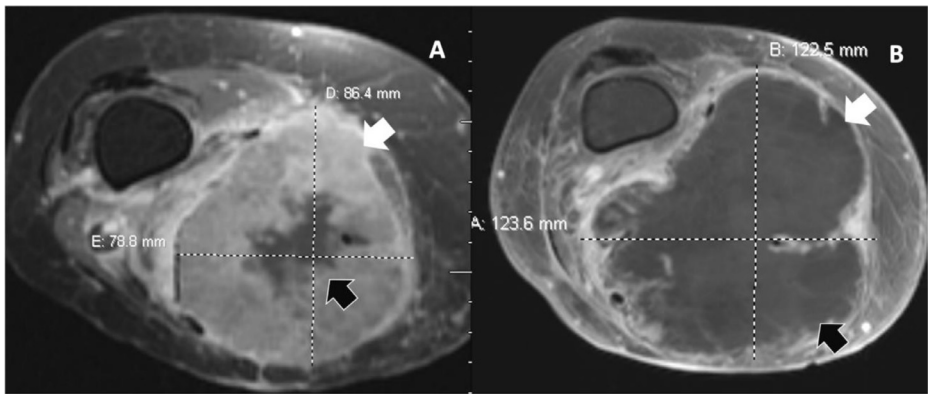

Figure 1 A 83-year-old woman with a high-grade unspecified pleomorphic sarcoma arising from the flexor compartment of the right thigh. (A) Axial fat saturated (FS) postintravenous gadolinium contrast (all contrast in the article is gadolinium-based unless stated otherwise) T1- weighted image (WI) demonstrates a heterogeneous soft tissue mass within the distal thigh, displaying thick peripheral solid enhancement (white arrow) and mild central necrosis (black arrow) before treatment. (B) Axial FS postcontrast T1-WI of the same tumor after chemo-radiation demonstrates increased size due to increased central necrosis (black arrow). The interval reduction of the peripheral solid enhancement (white arrow) indicates a positive response to therapy despite the increase in size. This phenomenon is termed "pseudoprogression."

Pseudoprogression may occur in the setting of targeted therapy as a response-related phenomena. It can be seen in lesions such as hepatocellular carcinoma (HCC), melanoma, and gastrointestinal stromal tumors (GIST), among others, and can be misjudged to be actual progression by size-based response criteria. Targeted anticancer therapy using antiangiogenic agents, such as tyrosine kinase inhibitors, is capable of causing this counterintuitive increase in tumor size because of drug-induced tumor hemorrhage or necrosis. The paradoxical enlargement can also be caused by immune-checkpoint inhibitors due to cytotoxic or vasogenic edema and inflammation with hemorrhage caused by the breakdown of tumor vasculature.[1] Pseudoprogression can occur following soft-tissue sarcoma treatment with neoadjuvant chemotherapy due to the induction of intralesional hemorrhage, typically causing enlargement of the central nonenhancing component with a reduction of solid enhancing areas (Fig. 1).[19, 20]

Pseudoprogression can occur following radiation therapy, often following a single or hypofractionated high dose. Common radiation therapy options include stereotactic radiosurgery (SRS) and stereotactic body radiotherapy (SBRT), which are stereotactic ablative radiotherapy (SABR) treatments and are an increasingly popular form of radiotherapy. SRS typically is used to treat brain lesions, and SBRT is defined as the treatment of extracranial tumors with a fractioned delivered dose, although it can be used to apply the entire dose in a single fraction. Spinal stereotactic radiosurgery (SSRS) and stereotactic spinal radiation therapy (SSRT) are similar. While SSRS delivers a large dose of radiation on a single day, SSRT is typically applied with a fractionated treatment schedule. Volumetric modulated arc therapy (VMAT) is a radiation therapy technique capable of achieving a highly conformal dose in comparison with conventional radiotherapy and is also capable of reducing the treatment delivery time compared with conventional static field intensity-modulated radiotherapy (IMRT).[21-23]

Soft-tissue tumors that receive preoperative radiotherapy may demonstrate significant contrast enhancement when histopathological examination reveals no viable tumor tissue. This phenomenon occurs in less than 10% of good responders and approximate 30% of patients with an intermediate response.[24] The tumor volume may increase in size during the postradiation period in up to 40% of cases. Additionally, changes in postradiation tumor volume may not correlate with the degree of tissue necrosis, as elucidated by Tsagozis et al (Fig. 2).[25]

Postradiation pseudoprogression can also occur following radiation therapy to spine metastases, particularly after single-fraction stereotactic radiosurgery. This phenomenon is known as "osseous pseudoprogression" and tends to occur between 3 and 6 months after therapy in as many as one-third of the cases.[24] As published by Chansik et al,[26] postradiation spinal tumor pseudoprogression was observed in 18% of treated spinal segments. Factors that helped to distinguish pseudoprogression from local recurrence included tumor enlargement within the 80% isodose line (the line encompassing an area surrounding the center of the radiating beam where the absorbed dose ranges in between 80% to 100% of the maximum beam dose), early enlargement (5 months for pseudoprogression vs 15 months for local recurrence), and increased T2-weighted signal intensity[27]. If a tumor demonstrates postradiation enlargement, careful assessment should take place to differentiate real progression from a form of pseudoprogression.[28]

Functional Assessment of Treatment Response in Targeted Therapy

Cancer immunotherapy using immune checkpoint inhibitors has become an effective treatment option for several advanced cancers. Due to the distinct mechanisms of

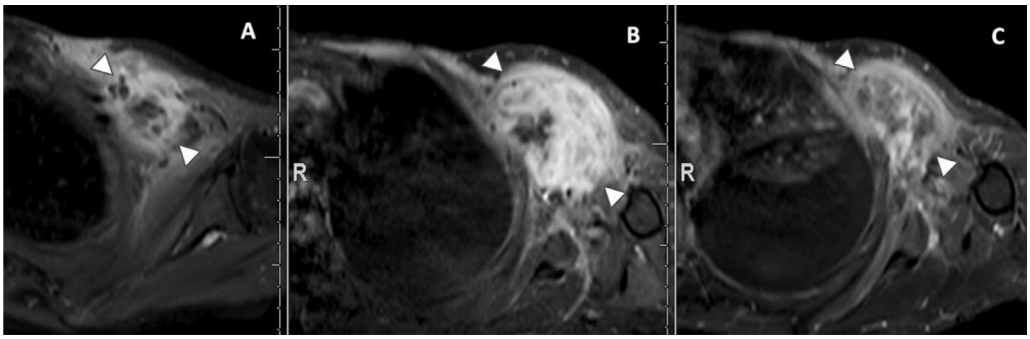

Figure 2 A 58-year-old man with a left pectoral myxoid pleomorphic soft tissue sarcoma. (A) Pretherapeutic axial FS T1 contrast enhanced MRI demonstrates a rim enhancing pectoral and axillary mass (double white arrowheads). (B) One-month postradiation therapy with volumetric modulated arc therapy (VMAT) of the left chest wall that delivered 45 Gy in 15 fractions. The axial FS T1 contrast enhanced image demonstrates increased size and enhancement (double white arrowheads). (C) Two months after VMAT, the axial FS T1 contrast enhanced image demonstrates decreased peripheral enhancement (double white arrowheads), indicative of a true positive response, preceded by post-radiation pseudoprogression in (B). The resected specimen demonstrated 95% necrosis, granulation tissue and no viable tumor.

immunotherapy that work by activating host immunity to treat cancers, numerous immune-related phenomena take place in terms of tumor response and progression as well as drug toxicity. The immune-related events can manifest as a broad spectrum of imaging findings in each organ. Although pseudoprogression has become an increasingly recognized phenomenon of immune-related tumor response, its incidence is low (10%). After treatment with immune-targeted therapies, different mechanisms can cause intralesional infiltration of immune cells into the tumor with an associated release of cytokines that can cause pseudoprogression due to associated cytotoxic edema or vasogenic edema, inflammation, and hemorrhage.[20]

The RECIST criteria are of great value due to the standardization of size metrics that provides interobserver reliability and facilitates data comparison from different trials. Nevertheless, the RECIST criteria are rather insensitive for the detection of very early response, and the criteria are incapable of characterizing lesion composition, viability and tumor-associated inflammation or immune cell infiltration. Targeted therapy can affect tumors by interacting with mechanisms such as angiogenesis, cell density and metabolism, signal pathways and immunity. Response from targeted and conventional therapies may be assessed by techniques such as DCE, DWI, and FDG-PET.

Particularly significant has been the role of targeted therapy in the treatment of advanced renal cell carcinoma (RCC). Several novel molecular targeted agents and immune checkpoint inhibitors are available for this purpose, including the 3 main classes of anticancer agents, including antiangiogenic agents, the mTOR (mammalian target of rapamycin) inhibitors, and immune modulators. Because the tumor burden (size) often remains stable for a prolonged period of time without significant shrinkage, less than one-half of RCC patients treated with targeted agents achieve an objective response according to RECIST. The reported response rates measured by the RECIST criteria range from 10% to 40% for VEGF-targeted therapies, and less than 10% for mTOR inhibitors. This phenomenon, labeled as a stable disease by RECIST, actually represents "clinical benefit,"[28] with improvement in progression-free survival (PFS) in both the first-line and second-line settings.[29]

Functional Multiparametric Assessment of Treatment Response in MSK oncology

The European Organization for Research and Treatment of Cancer (EORTC) Guidelines express the utility of some of the most accepted functional imaging modalities, including PET, MR spectroscopy (MRS), DWI, and DCE-CT in cancer imaging. Suggested guidelines include the use of the PET Response Criteria in Solid Tumors, Version 1.0 (PERCIST),[30] with diffusion-weighted MRI. An increase in ADC value in response to treatment is associated with a better outcome. Among the different imaging biomarkers of angiogenesis, dynamic DCE-MRI is capable of reliably representing angiogenesis as a crucial step for tumor growth and metastasis. Thus, it is often capable of measuring the therapeutic effect of VEGF inhibitors.[3] A caveat is that short-term imaging effects may not translate into increased overall survival and specific studies that correlate with overall survival are needed.

Bone and soft tissue sarcomas are a diverse group of malignant neoplasms that are derived from the connective tissues. More than 12 families of soft tissue sarcomas and 12 families of bone sarcomas exist in the 2013 WHO Classification of Tumors of Soft Tissue and Bone.[31] Certain types of sarcomas, such as monophasic synovial sarcoma and Ewing sarcoma, are composed principally of malignant cells. In contrast, other types can exhibit varying degrees of cellularity, such as lesions that form myxoid or chondroid stroma in addition to other substances such as fibrous septae and necrosis. Intratumoral hemorrhage, inflammatory infiltrates, and cystic degeneration can also contribute to the internal composition and size of sarcomas. While the neoplastic cells may be effectively eradicated by therapy, they may not constitute enough of the volume of the mass to impact overall size enough to be

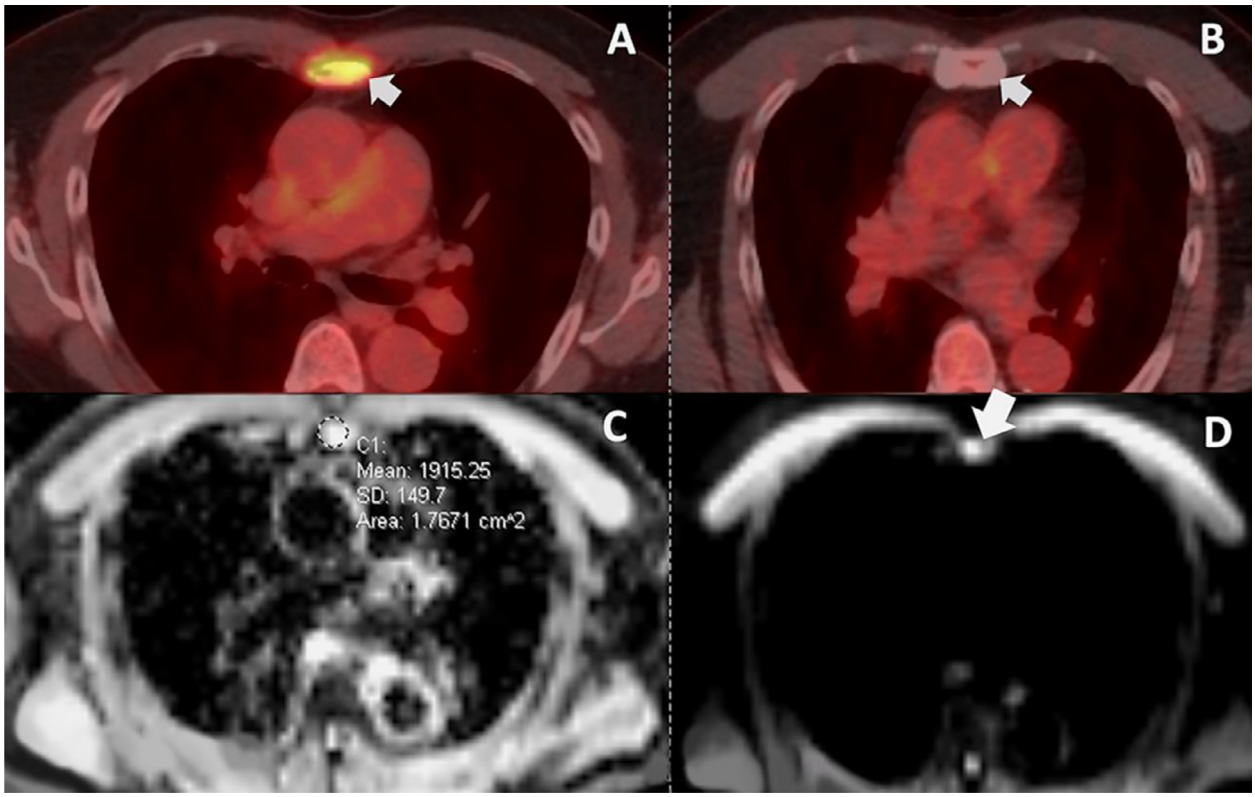

Figure 3 A 72-year-old man with multiple myeloma. (A) Fused axial pretreatment FDG PET/CT demonstrates an avid lesion in the sternum (small arrow). (B) Fused axial post-treatment FDG PET/CT demonstrates metabolic normalization (small arrow). (C) Axial post-treatment ADC map demonstrates a nonrestricting lesion displaying a mean ADC of 1.9×10^{-3} mm^2/s (circular region of interest (ROI)), that is consistent with granulation tissue and positive therapeutic response. (D) Axial post-treatment DWI displays a hyperintense lesion (large arrow) without corresponding ADC restriction (as demonstrated in C). The PET/CT and DWI/ADC findings are indicative of an interval positive treatment response.

accurately assessed by the RECIST criteria. This may explain why the RECIST criteria have a weak correlation with the prognosis in sarcoma patients.[32]

Functional MRI can be used to complement morphological imaging, thereby improving tissue characterization and the staging of bone and soft-tissue tumors.[33] The addition of functional MR sequences to conventional MR protocols may increase the sensitivity of MR imaging for determining treatment response in soft tissue sarcomas, particularly when the tumor forms granulation tissue and fibrosis rather than necrosis following neoplastic cell kill. Increasingly popular techniques include the assessment of ADC values and changes in vascular perfusion.[34] The use of combined diffusion and perfusion analysis can accurately portray the degree of treatment effect in soft tissue sarcoma patients following preoperative neoadjuvant systemic therapy. Response to treatment can be predicted with high specificity when no more than 5% of the entire treated soft-tissue sarcoma volume demonstrates both early arterial-like enhancement during DCE-MR, and ADC values below 1.0×10^{-3} mm^2/s as suggested by Soldatos et al.[35] These results suggest potential clinical utility even in the setting of a single preoperative MR scan performed after neoadjuvant treatment (please see the section on Perfusion in MSK Tumors for further information).

Multiparametric combined analysis using PET/MR scanning can be useful in predicting early therapeutic response by demonstrating an interval increase in ADC values parallel to a decrease in maximum standard uptake (SUV_{max}) (Fig. 3).[6]

Analysis with FDG PET/CT and postcontrast volumetric MR has also served to improve the differentiation of effective treatment response from disease progression when compared with the conventional RECIST criteria in Ewing sarcoma. Similarly, combined tumoral ADC assessment and FDG uptake distribution, when obtained before radiotherapy can aid treatment planning including dose escalation.[36] These techniques can also be useful for treatment response assessment in various soft-tissue sarcomas of the extremities.[37]

Understanding Functional Imaging in MSK Oncology: Advanced Bone and Soft Tissue Tumor Imaging (ABASTI)

DWI for the Characterization of MSK Lesions

Functional MRI can be used to complement morphological imaging.[38,39] DWI is a nonenhanced functional MRI technique that is easily incorporated into routine MRI protocols

with little additional scanning time, offering useful information regarding the cellularity of musculoskeletal and other lesions. Whole-body (WB) DWI has been studied for tumor detection, and localized DWI is a useful technique for characterizing lesions and assessing treatment response. DWI provides insight into tissue structure and organization as well as the orientation of molecular motion. The amount of signal loss from free diffusion is quantified as the ADC. Protons in a more restricted, densely cellular environment exhibit less signal loss than do freely mobile protons (as can be seen with cell necrosis following effective therapy) and therefore have comparatively lower ADC values.[39] A useful generalization for the interpretation of the signal intensity patterns on the diffusion sequences and ADC maps is that the combination of high signal on DWI with low signal on ADC maps indicates high tumor cellularity with intact, viable cell membranes that restrict the fluid. This pattern is found most commonly in malignant tumors (Fig. 4).

Low signal on DWI and low signal on ADC typically indicates fibrosis. On the other hand, a combination of high signal on DWI and high signal on ADC may be observed in cysts and hemangiomas, indicating a T2 shine-through effect. High signal on DWI and ADC may also indicate edema. Caution is advised as high signal on DWI, and high signal on ADC may also occur in viable tumors with high water content such as myxoid and chondroid lesions, including malignancies.[34,39] Noteworthy is that some of the highest ADC values found in sarcomas occurs in myxoid or chondroid lesions such as myxoid liposarcoma and mesenchymal chondrosarcoma (Fig. 5). However, the change in ADC upon comparison of pre- and post-therapeutic values can be predictive of response in a variety of tumors even though absolute values may be variable. Absolute quantification of ADC values can vary between scanners, thus, it is best to image the patient in the same scanner before and after therapy.

Since myxoid matrix results in increased ADC values due to the high water and mucin content, there is considerable overlap between the ADC values of benign and malignant myxoid tumors, and they should be considered separately from nonmyxoid lesions. In the case series presented by Khedr et al,[40] ADC measurements in benign skeletal tumors averaged $1.86 \pm 0.67 \times 10^{-3}$ mm^2/s, ranging from 0.4×10^{-3} mm^2/s in aggressive fibromatoses to 2.6×10^{-3} mm^2/s in juxtacortical chondromas. Malignant tumors averaged $0.97 \pm 0.35 \times 10^{-3}$ mm^2/s, ranging from 0.81×10^{-3} mm^2/s in malignant fibrous histiocytoma to 2.1×10^{-3} mm^2/s in mesenchymal chondrosarcoma (Fig. 6).[40]

DWI can help distinguish between tumors with different prognoses but overlapping anatomic imaging features, such as the case of chordoma versus chondrosarcoma of the skull base. Chondrosarcoma with a large amount of chondroid stroma is associated with a high mean ADC value (2.0×10^{-3} mm^2/s) that is significantly different from classic chordoma (1.4×10^{-3} mm^2/s) and poorly differentiated

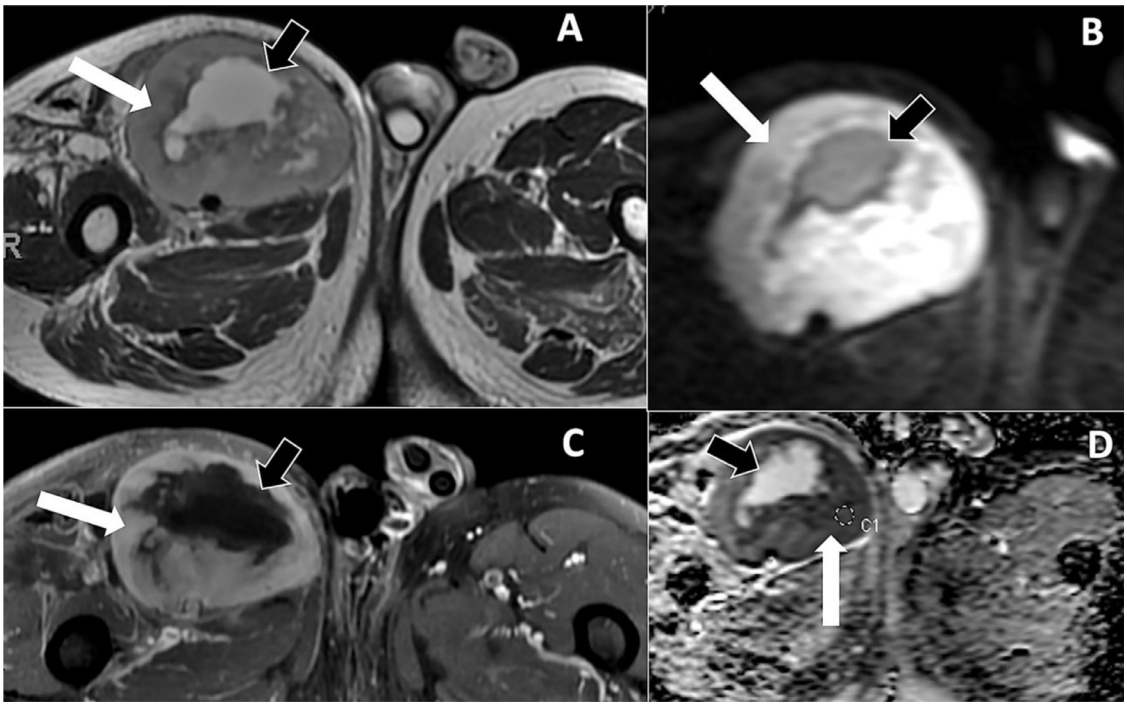

Figure 4 A 73−year-old man with a dedifferentiated liposarcoma in the proximal right thigh. (A) Axial T2-WI demonstrates an area of central T2 hyperintense liquefactive necrosis (black arrow) surrounded by a nodular rim of solid tumor (white arrow). (B) Axial DWI demonstrates signal that is higher in the solid component (white arrow) than in the central necrosis (black arrow). (C) Axial FS T1 post contrast sequence demonstrates enhancement of the solid peripheral component. (D) ADC map demonstrates restricted diffusion within the solid component (white arrow), with an ADC value of 0.9×10^{-3} mm^2/s (ROI), indicative of a viable tumor component with high cellularity at the periphery but not the center of the lesion (black arrow).

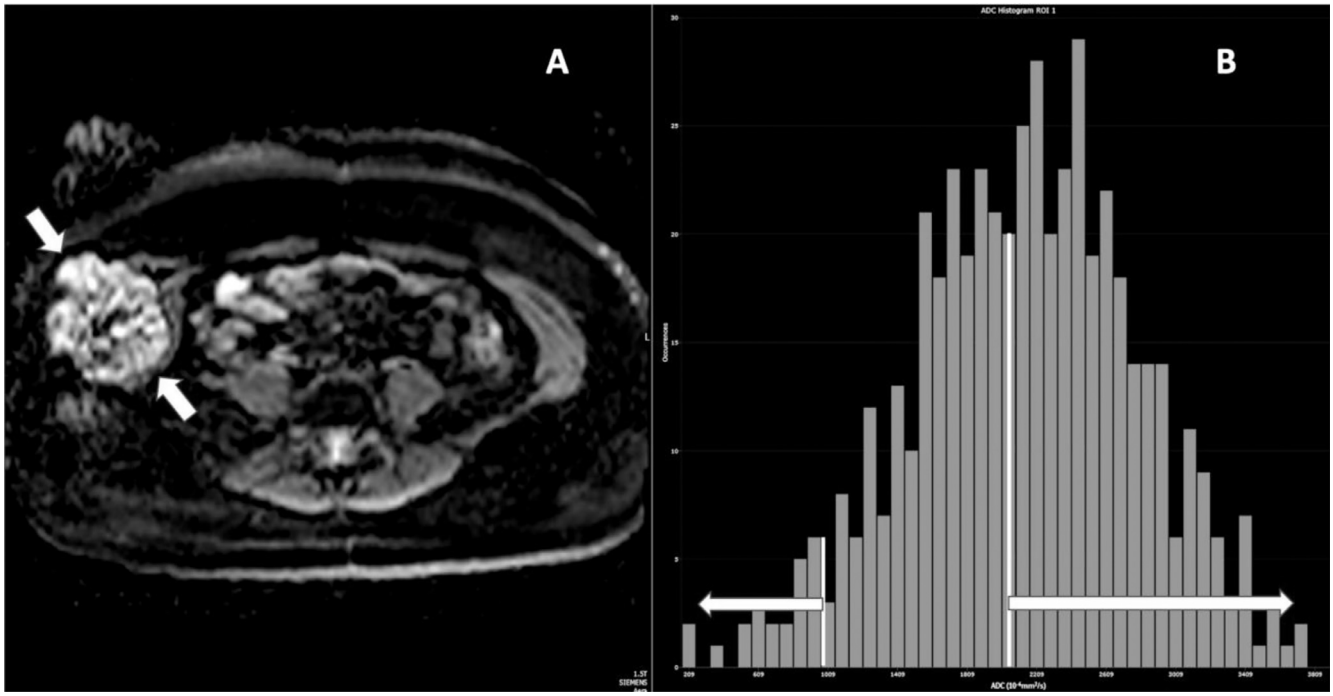

Figure 5 A 54-year-old woman with high-grade chondrosarcoma arising from the right iliac bone. (A) Axial ADC map demonstrates high signal (white arrows) due to its water and protein-rich matrix despite malignant histology. The high ADC values overlap with benign tumors. (B) ADC histogram demonstrates that a large proportion of the tumor pixels concentrate in values above 2.0×10^{-3} mm^2/s (arrow pointing toward the right), (chondroid and myxoid tissue), and a small proportion of pixels demonstrate ADC values under 1.0×10^{-3} mm^2/s (high-grade cellular tumor), (arrow pointing towards the left).

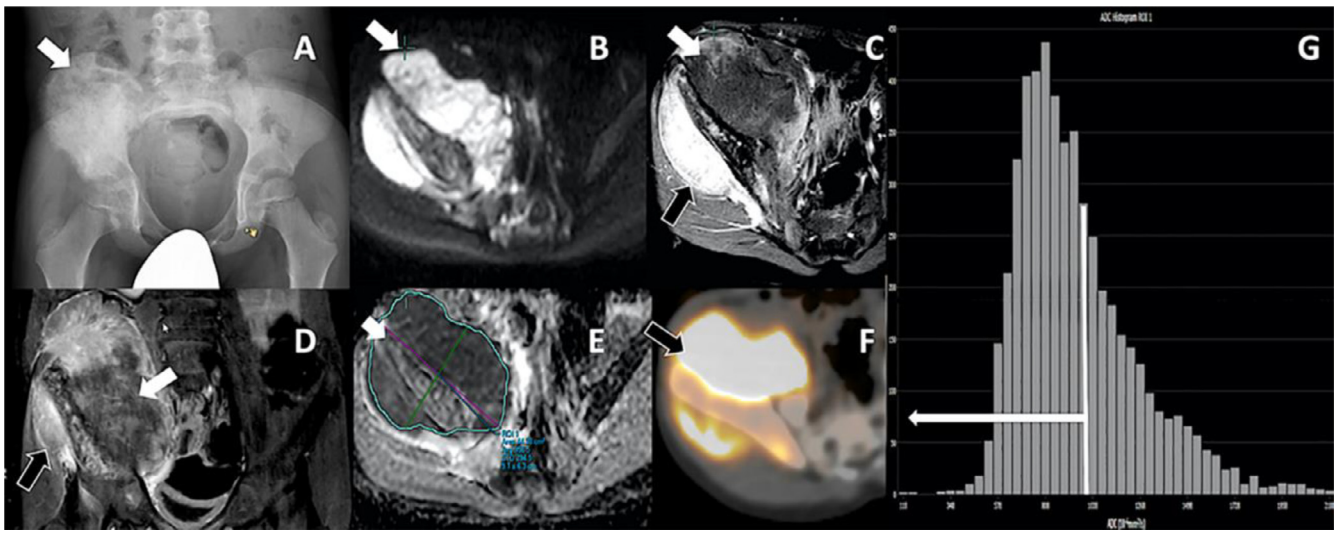

Figure 6 A 7-year-old girl with high-grade conventional osteosarcoma arising from the right iliac bone. (A) AP radiograph of the pelvis demonstrates a large osteoid-producing tumor in the right iliac wing (white arrow). (B) Axial DWI demonstrates tumor with high signal intensity (white arrow). Axial (C) and coronal (D) FS T1 contrast-enhanced sequences demonstrate peripheral enhancement and an artifactual anterior lack of enhancement in a heavily calcified area (pseudonecrosis, white arrows). The posterior aspect of the tumor is less heavily mineralized and demonstrates expected enhancement (black arrows). ADC map (E) demonstrates significant restriction across the tumor, with an average value of 0.9×10^{-3} mm^2/s (ROI — small arrow), consistent with cell viability. (F) The tumor displays high FDG avidity on PET/CT, an additional sign of viability (black arrow) including the area of anterior "pseudonecrosis" seen in (C-D). Furthermore, (G) the ADC histogram demonstrates that a significant proportion of tumor pixels are concentrated below 1.0×10^{-3} mm^2/s (white arrow pointing towards the left), reflecting the high cellularity of the viable malignancy. (Color version of figure is available online.)

chordoma (0.875×10^{-3} mm^2/s), ($P < 0.001$), as presented by K.W. Yeom et al.[41] Both skull base tumors are malignant, although with different levels of aggressiveness. Although both demonstrate high ADC values that overlap with benign tumors, their average ADC values are different enough to allow separation from each other in the context of the 2 most common tumors arising from the skull base.

Caution is advised when interpreting the ADC maps of solid soft tissue masses with values lower than simple fluid collections. For example, hematomas may demonstrate low ADC values because of susceptibility related T2* shortening and T2 shading that affect the signal intensity on DWI. Erroneous diagnoses of malignant tumors can occur when the determination is based on restricted diffusion when in the presence of blood, melanin, high-protein content, and iron because these substances may lead to nontumoral restricted diffusion.[42]

Typical spinal marrow ADC values in children and young adults have a value of approximately 0.5×10^{-3} mm^2/s. As people age and the bone marrow increases in fat content, the normal ADC value drops closer to 0.4×10^{-3} mm^2/s. Most cellular malignant tumor components demonstrate ADC values ranging between 0.7 and 1.0×10^{-3} mm^2/s. Therefore, the interpretation of DWI in the marrow cavity of bone differs from soft tissue lesions because the low ADC value of yellow marrow fat contributes to the value of the ROI and lowers it. Therefore, the ADC values of hypercellular and malignant lesions in the soft tissues are often higher than those that arise in yellow marrow. When bone metastases are treated, over time, they can redevelop yellow marrow that replaces the pre-existing tumor, leading to post-therapeutic ADC measurements below the pretherapeutic values. This counterintuitive lowering of ADC values is a sign of positive response in the marrow cavity of adults.[39]

Messiou et al[33] concluded that the post-therapeutic increase in sclerosis in bone metastases from prostate cancer following effective treatment does not significantly impede diffusion. They found no significant correlation between changes in ADC and Hounsfield unit (absorption/attenuation coefficient of radiation within a tissue used during CT reconstruction) measurement. This finding is in contradistinction to the notion that increasing sclerosis would inhibit ADC

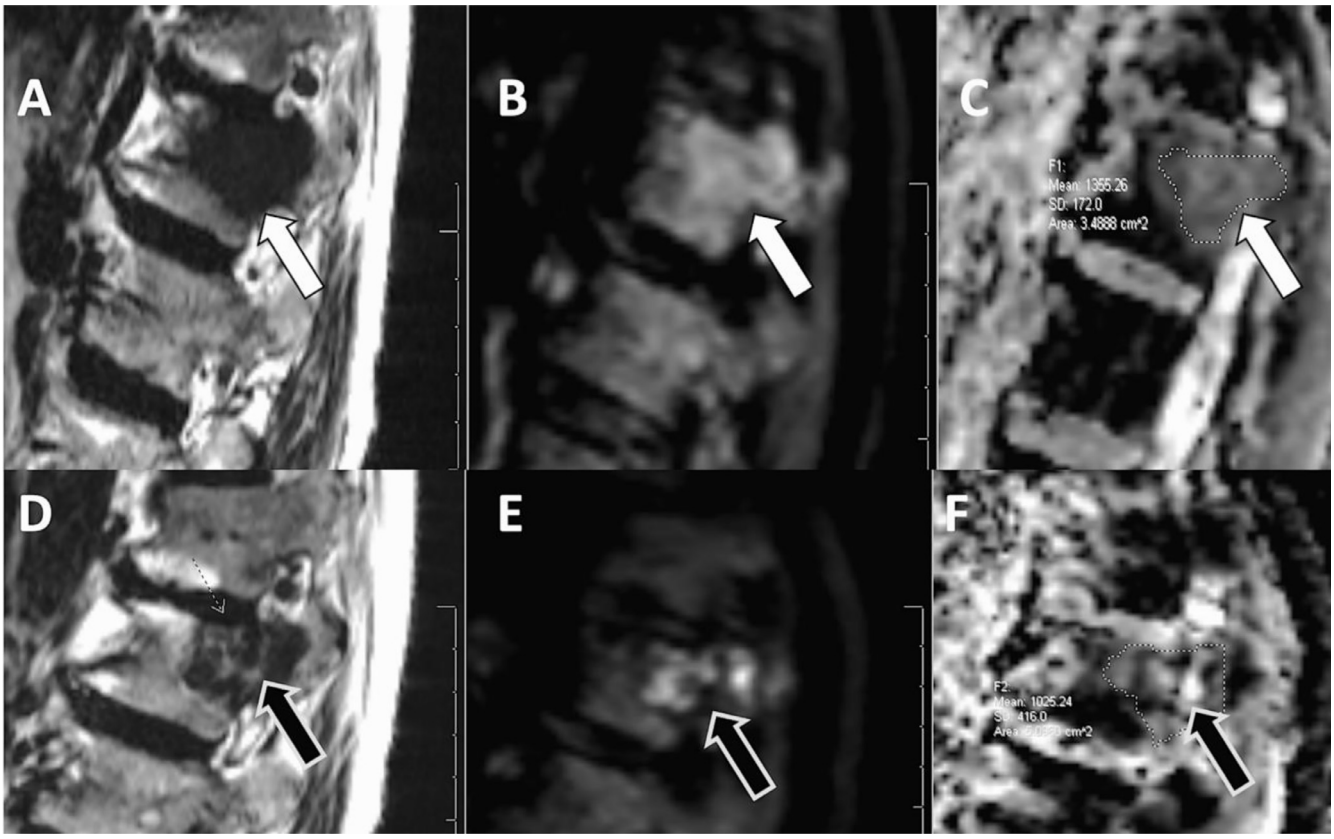

Figure 7 A 72 -year-old woman with metastatic rectal adenocarcinoma receiving treatment with cetuximab with irinotecan. After 7 months of systemic treatment, (A) sagittal T2 Dixon fat-only sequence demonstrates marrow replacement within the L1 vertebral body and right pedicle (white arrow). (B) Sagittal DWI (b value 800) sequence demonstrates mild diffusion restriction (white arrow). (C) Sagittal ADC map demonstrates an average ADC value of 1.3×10^{-3} mm^2/s, indicating treatment effect (higher ADC than expected in the nontreated tumor), (white arrow). After 9 months of treatment, (D) sagittal T2 Dixon fat-only sequence demonstrates partial yellow marrow reconversion within the lesion, indicative of positive treatment effect (arrows). (E) Small areas of T2 shine through without significant diffusion restriction are observed on DWI, which is the typical appearance of treatment effect (black arrow). (F) The partial yellow marrow reconversion causes an overall paradoxical reduction of the ADC of the lesion, now 1.0×10^{-3} mm^2/s (black arrow).

assessment, a concept is at least partially based on published evidence indicating that predominantly osteolytic metastases have a significantly higher ADC than sclerotic metastases.[43] However, when Hounsfield units increase by more than 50%, there tends to be a simultaneous rise in the ADC values, which is typically accepted as a sign of positive treatment response. Therefore, the notion that increased bone sclerosis in responding patients occurs in concordance with rising ADC values needs to be further validated by more extensive study series.

DWI can estimate residual tumor activity after treatment and help to detect recurrences at an early stage, often when curative treatment is still possible. Differentiating treatment-related tissue changes from a residual or recurrent tumor is a common problem, given the lack of specificity of signal abnormalities on standard MRI (such as a low signal on T1-weighted images, high signal on T2-weighted images and enhancement following contrast administration). Post therapeutically, when compared with conventional, static, contrast-enhanced studies, DWI is expected to more readily help differentiate areas of granulation tissue and scarring from areas of viable cellular tumor. In patients with osteosarcoma and Ewing sarcoma, the change in mean ADC values showed a statistically significant difference between good and inadequate response to neoadjuvant chemotherapy.[40] Necrosis in osteosarcomas results in high ADC values. Both the minimum and the mean ADC values of osteosarcomas are significantly increased after effective chemotherapy when compared to baseline. Even minimum ADC values are considerably higher in good responders (>90% of necrosis by histological examination) than in poor responders.[38]

Whole tumor (WT) ADC histograms represent the distribution of ADC values throughout the tumor. Most malignant tumor components tend to demonstrate a concentration of pixels with ADC values of 1.0×10^{-3} mm^2/s or less (the left portion of the distribution histogram curves such as in Figs. 5 and 6). Benign tumor components, as well as areas responding to treatment, tend to demonstrate higher ADC values (right side of the histogram curves). Exceptions to this tendency include malignant tumors with intrinsically high ADC values such as chondroid and myxoid tumors and, on the other hand, benign tumors with low ADC values such as mature desmoid tumors (Fig. 7).[40] Typically, a post-treatment displacement of the histogram to the right indicates decreased cellularity and positive treatment response (Fig. 8).[44]

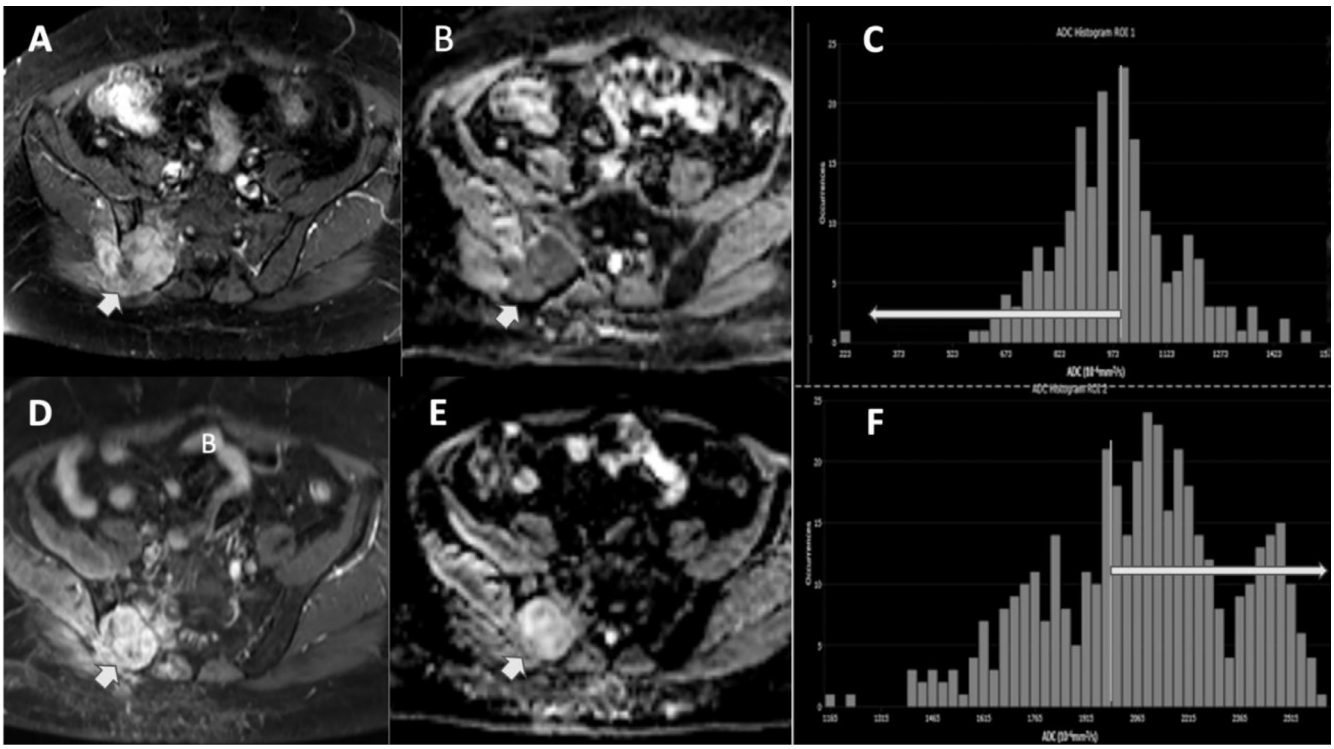

Figure 8 A 55-year-old woman with metastatic uterine leiomyosarcoma. (A) Axial FS T1 postcontrast image obtained before stereotactic spine radiation therapy (SSRS), demonstrates an enhancing metastasis within the right iliac bone (white arrow). (B) ADC map shows tumor diffusion restriction with an ADC average of 0.9×10^{-3} mm^2/s (white arrow). (C) ADC histogram demonstrates that most tumor pixels are below 1.0×10^{-3} mm^2/s indicating a viable cellular tumor with intact cell membranes resulting in low diffusion (white arrow pointing to the left). (D) After SSRS, the axial FS T1 postcontrast image demonstrates mild interval size-reduction, with a relatively unchanged amount of enhancement. (E) ADC map no longer demonstrates tumor diffusion restriction with an ADC average of 2.1×10^{-3} mm^2/s (white arrow). (F) ADC histogram shows that most of the tumor pixels are now situated above an ADC value of 2.0×10^{-3} mm^2/s (white arrow now pointing to the right) indicative of a positive treatment response regardless of relative stable tumor size and enhancement as demonstrated in (D).

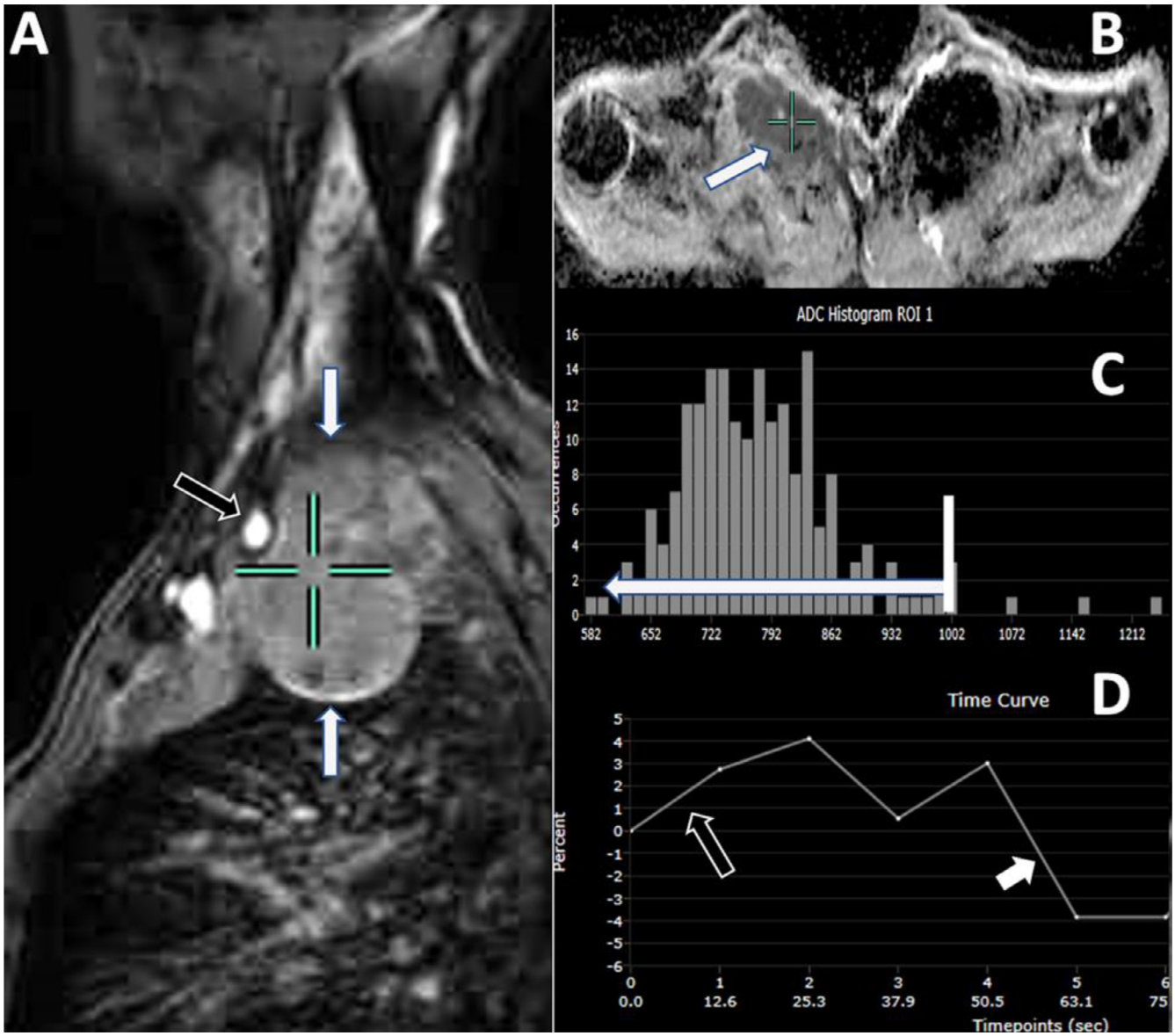

Figure 9 A 45-year-old man with an untreated metastasic prostatic adenocarcinoma with neuroendocrine features. (A) Sagittal postcontrast 3D volumetric interpolated breath-hold examination (VIBE) sequence demonstrates a lobulated mass centered in the superior sulcus of the right lung (white arrows) displaying early arterial enhancement (black arrow showing arterial phase enhancement in the subclavian artery). (B) Axial ADC map demonstrates that the mass displays homogenous diffusion restriction (white arrow) with a mean ADC value of 0.7×10^{-3} mm^2/s. (C) ADC histogram shows that most tumor pixels are centered in between 0.6 and 0.8×10^{-3} mm^2/s (malignant cellular tumor), with almost all pixels below the ADC value of 1.0×10^{-3} mm^2/s (white arrow pointing toward the left). (D) Contrast-enhanced dynamic perfusion (PWI/DCE) sequence, demonstrates a Type 3 curve with rapid wash-in (black arrow) followed by wash-out (white arrow). Both of these ADC and PWI/DCE features are commonly found in cellular high-grade viable malignant tumors. (Color version of figure is available online.)

The use of ADC histograms has proven useful in differentiating benign from malignant pancreatic and adrenal tumors, in separating neurogenic tumors from sarcomas, and in identifying malignancies such as diffuse pontine gliomas, cervical carcinomas, and myeloma.[45-49] In a study published by Bharwani et al,[50] diffusion-weighted and ADC tumor histogram analysis was used to measure the response to neoadjuvant sunitinib in metastatic renal cell carcinoma. Their study demonstrated that patients in whom the tumor ADC histogram showed a higher number of pixels contained within the lowest 25th percentile values at baseline (left portion of the distribution histogram curve), demonstrated a reduced overall survival.

Perfusion in MSK Tumors

The most common forms of contrast-based PWI are T2*-weighted dynamic susceptibility contrast (DSC) perfusion and T1-weighted DCE perfusion. Arterial spin labeling (ASL) is a noncontrast perfusion technique that measures flow by

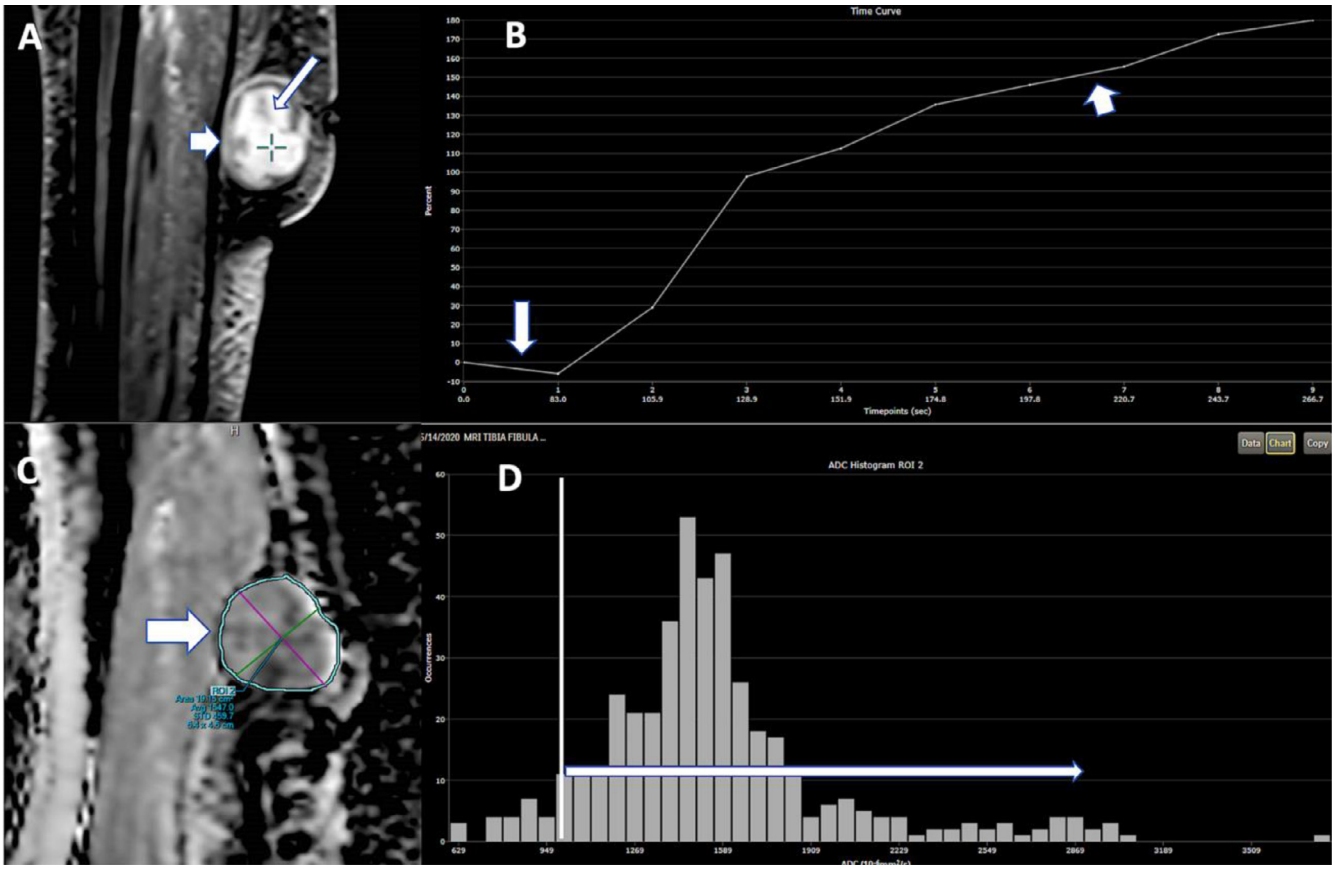

Figure 10 A 65-year-old woman with an untreated benign nerve sheath tumor (schwannoma). (A) Sagittal postcontrast 3D VIBE sequence demonstrates an ovoid-shaped tumor in the posterior left calf (short arrow), displaying central enhancement (long arrow). (B) Contrast-enhanced dynamic perfusion (PWI/DCE) sequence, demonstrates a type 1 curve without rapid arterial enhancement (arrow pointing down) followed by sustained wash-in (arrow pointing up). (C) Sagittal ADC map demonstrates that the mass displays heterogeneous diffusion (arrow) with a mean ADC value of 1.5×10^{-3} mm^2/s. (D) ADC Histogram demonstrates that almost all tumor pixels above 1.0×10^{-3} mm^2/s (benign tumor). Both of these ADC and PWI/DCE features are common in benign tumors. (Color version of figure is available online.)

applying a tagging pulse to the inflowing blood proximal to the targeted imaged area.[51] In musculoskeletal imaging, the most commonly utilized form of PWI is DCE. Qualitative analysis with PWI, using the DCE technique shows the presence of progressive enhancement, delayed plateau, or delayed wash-out of contrast in tumors, resulting in time-intensity curves that separate kinetic curve morphologies into 3 primary groups; Type I (slow continuous upslope), Type II (rapid upslope followed by a plateau) and Type III (rapid upslope followed by wash-out). This analysis of the nature of the contrast enhancement can help with benign-malignant soft tissue tumor differentiation. As presented by Yildirim et al,[52] most malignant tumors demonstrated Type 2 or Type 3 curves (Fig. 9), while the Type 1 curve was seen mostly among benign tumors (Fig 10).

A more detailed time-signal curve classification that is most commonly used in applications for whole spine perfusion and myeloma includes a Type 1 curve indicating no enhancement, a Type 2 curve demonstrating slow, sustained enhancement, a Type 3 curve with fast and steep first-pass enhancement followed by sustained late enhancement, a Type 4 curve showing a steep slope, followed by washout of contrast medium, and a Type 5 curve showing fast and steep enhancement, followed by stable late enhancement. The Type 4 kinetic curve is caused by the small interstitial compartment that corresponds to the high cellularity and best correlates with viable malignancy.[53]

Perfusion-weighted imaging and particularly tumor kinetic assessment with DCE using dynamic gadolinium injection and enhancement time-intensity curve analysis has proven useful in evaluating treatment response in tumors where response underestimation may occur with the use of size-based traditional evaluation.[1] Dynamic perfusion MRI can also help estimate response to preoperative chemotherapy. Following therapy for soft tissue sarcomas, foci of early and rapidly progressive enhancement are indicative of residual or recurrent tumor, whereas the absence of early enhancement indicates a good response. Good and poor responders can be separated based on first-pass subtraction images or enhancement time-intensity curves. Recurrent bone tumors (except for cartilaginous components) exhibit earlier and faster enhancement as compared to healthy reference tissue.[34]

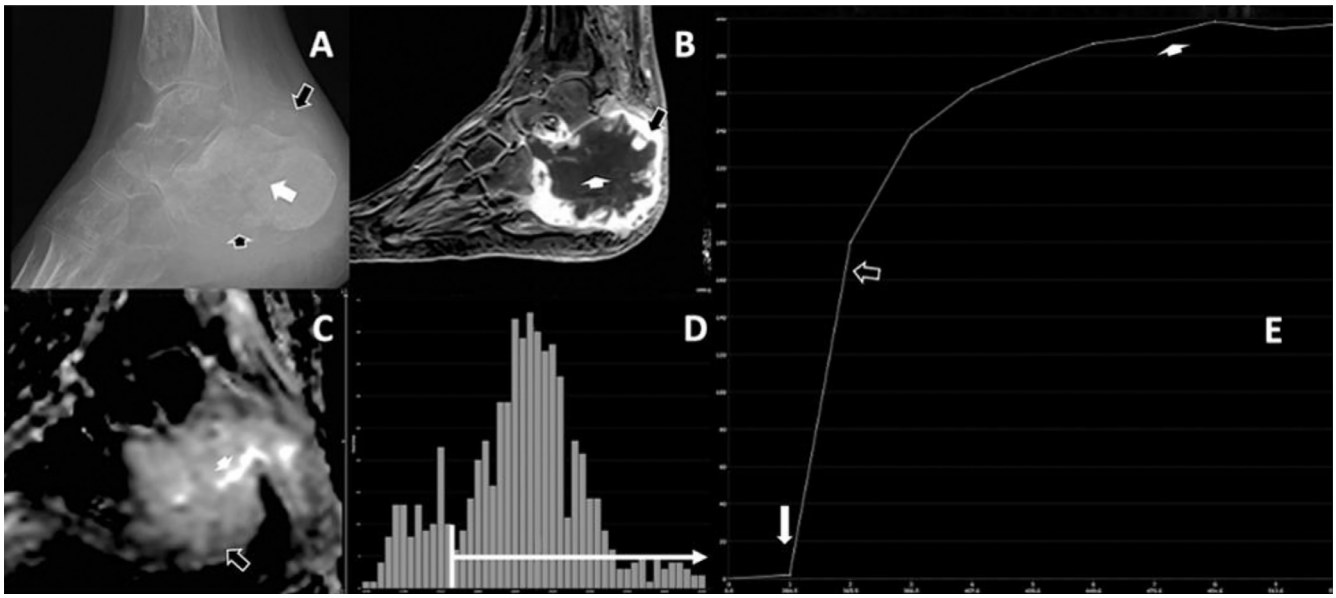

Figure 11 A 37-year-old man with a high-grade chondroblastic osteosarcoma arising from the left calcaneus, after systemic chemotherapy with cisplatin and doxorubicin. (A) Lateral ankle radiograph demonstrates fracture and osteolytic destruction of the calcaneus (white arrow), tumor osteoid (small black arrow), and soft-tissue mass (large black arrow). (B) Sagittal FS T1 contrast-enhanced image demonstrates rim enhancement (black arrow) with central necrosis (small white arrow). (C) The ADC map demonstrates high signal central necrosis (short white arrow), with an ADC of 3.3×10^{-3} mm^2/s and a solid peripheral component with lower ADC values (black arrow), ranging from 1.4-2.3×10^{-3} mm^2/s (consistent with granulation tissue). (D) ADC histogram demonstrates that a significant proportion of the tumor pixels are above 2.0 (granulation tissue and necrosis), (white arrow pointing towards the right) and particularly between 2.2 and 2.6×10^{-3} mm^2/s. (E) Postcontrast DCE PWI kinetics demonstrates a Type 3 curve without early arterial fast wash-in (long white arrow), a continuous up-slope (black arrow) and a late plateau, without a late wash-out (small white arrow).

DCE-MRI has been utilized for the assessment of spinal metastatic sarcoma 2 months after treatment with stereotactic body radiation therapy, providing an excellent correlation to local control. Traditional analysis based on size criteria alone is less able to judge ultimate disease progression.[54] DCE perfusion imaging has been successfully used to monitor response in MR—guided focused ultrasound for the treatment of bone metastasis obtained at 3 months follow-up. A study has revealed that the absence of central perfusion indicates that the neoplastic tissue has been replaced by necrosis. A rim of persistent contrast uptake at the periphery of the lesion on conventional imaging is indicative of a hyperemic reactive layer caused by high local temperature during treatment rather than residual tumor.[55] PWI, DCE imaging can help to identify tumor enhancement due to therapeutic effect rather than viable malignant cells (Fig. 11).

Conclusion

As oncologic treatment shifts from conventional systemic and radiation therapy into advanced targeted forms of therapy that are capable of extending patient survival but not necessary reducing the size of tumors, new metrics other than size-based criteria are gaining greater relevance. New imaging methods such as DWI and PWI are providing more accurate indicators of the true nature of tumor behavior. These techniques can help to resolve common diagnostic dilemmas such as identifying tumor expansion due to post-therapeutic necrosis rather than disease progression, and distinguishing granulation tissue from recurrent tumor. Adding to anatomic evaluation, these new functional modalities have the potential to improve therapeutic response assessment.

References

1. Nishino M, Hatabu H, Stephen Hodi F: Imaging of cancer immunotherapy: Current approaches and future directions. Radiology 290:9-22, 2019
2. Eisenhauer EA, Therasse P, Bogaerts J, et al: New response evaluation criteria in solid tumors: Revised RECIST guideline (version 1.1) E.A. Eur J Cancer 4 5:228-247, 2009
3. Nishino M, Jagannathan JP, Ramaiya NH, et al: Revised RECIST guideline version I.I: What oncologist want to know and what radiologist need to know. AJR 195:281-289, 2010.. 2-A Radiologist's Guide to Treatment Response
4. Schuetze SM, Baker LH, Benjamin RS, et al: Selection of response criteria for clinical trials of sarcoma treatment. Oncologist 13(suppl 2):32-40, 2008
5. Choi H, Charnsangavej C, de Castro Faria S, et al: CT evaluation of the response of gastrointestinal stromal tumors after imatinib mesylate treatment: A quantitative analysis correlated with FDG PET findings. AJR 183:1619-1628, 2004
6. Bruix J, Sherman M, Llovet JM, et al: Clinical management of hepatocellular carcinoma: conclusions of the Barcelona-2000 EASL conference. European Association for the Study of the Liver. J Hepatol 35:421-430, 2001

7. Gerwing M, Herrmann K, Helfen A, et al: The beginning of the end for conventional RECIST — Novel therapies require novel imaging approaches. Nature reviews. Clin Oncol 16:442-458, 2019
8. Rezai P, Pisaneschi M, Feng C, et al: Criteria in oncologic imaging: Functional, molecular, and disease-specific imaging biomarkers. AJR 201:246-256, 2013
9. Cheson BD, Pfistner B, Juweid ME, et al: Revised response criteria for malignant lymphoma. J Clin Oncol 25:579-586, 2007
10. Smith AD, Lieber ML, Shah SN: Assessing tumor response and detecting recurrence in metastatic renal cell carcinoma on targeted therapy: The importance of size and attenuation on contrast-enhanced CT. AJR 194:157-165, 2010
11. Smith AD, Shah SN, Rini BI, et al: Morphology, Attenuation, Size, and Structure (MASS) criteria: Assessing response and predicting clinical outcome in metastatic renal cell carcinoma on antiangiogenic targeted therapy. AJR 194:1470-1478, 2010
12. Wen PY, Macdonald DR, Reardon DA, et al: Updated response assessment criteria for high-grade gliomas: Response assessment in the neuro-oncology working group. J Clin Oncol 28:1963-1972, 2010
13. Costelloe CM, Chuang HH, Madewell JE, et al: Cancer response criteria and bone metastases: RECIST 1.1, MDA, and PERCIST. J Cancer: 1, 2010
14. Hamaoka T, Madewell JE, Podoloff DA, et al: Bone imaging in metastatic breast cancer. J Clin Oncol 22:2942-2953, 2004
15. Hayashi N, Costelloe CM, Hamaoka T, et al: A prospective study of bone tumor response assessment in metastatic breast cancer. Clin Breast Cancer 13(1):24-30, 2013
16. Niikura N, Liu J, Costelloe CM, et al: Initial staging impact of fluorodeoxyglucose positron emission tomography/computed tomography in locally advanced breast cancer. Oncologist 16:772-782, 2011
17. Costelloe CM, Ueno. NT, Lin PP, et al: Bone Metastases. Oncologic Imaging: A Multidisciplinary Approach. Elsevier, 591-609, 2012
18. McDonald R, Probyn L, Poon I, et al: Tumor response after stereotactic body radiation therapy to nonspine bone metastases: An evaluation of response criteria. Int J Radiat Oncol Biol Phys 93(4):879-881, 2015
19. Varma DG, Jackson EF, Pollock RE, et al: Soft-tissue sarcoma of the extremities: MR appearance of post-treatment changes and local recurrence. Magn Reson Imaging Clin N Am 3:695-710, 1995
20. Garner HW, Kransdorf MJ, Bancroft LW, et al: Benign and malignant soft-tissue tumors: Posttreatment MR imaging. RadioGraphics 29:119-134, 2009
21. Brown M, Carlson DJ, Brenner DJ: The tumor radiobiology of SRS and SBRT: Are more than the 5 R's involved? J Int J Radiat Oncol Biol Phys 88:254-262, 2014
22. Teoh M, Clark CH, Wood K, et al: Volumetric modulated arc therapy: A review of current literature and clinical use in practice. Br J Radiol 84:967-996, 2011
23. Einarsdottir H, Wejde J, Bauer H: Preoperative radiotherapy in soft tissue tumors: Assessment of response by static post-contrast MR imaging compared to histopathology. Acta Radiologica 42(1):1-5, 2001
24. Amini B, Beaman CB, Madewell JE, et al: Osseous pseudoprogression in vertebral bodies treated with stereotactic radiosurgery: A secondary analysis of prospective phase I/II clinical trials. AJNR Am J Neuroradiol 37:387-392, 2016
25. Tsagozis P, Brosjo O, Skorpil M: Preoperative radiotherapy of soft tissue sarcomas: Surgical and radiologic parameters associated with local control and survival. Clin Sarcoma Res 8:19, 2018
26. Bahig H, Simard D, Létourneau L, et al: A study of pseudoprogression after spine stereotactic body radiation therapy. Int J Radiation Oncol Biol Phys 96(4):848-856, 2016
27. Wortman JR, Tirumani SH, Jagannathan JP, et al: Radiation therapy for soft-tissue sarcomas: A primer for radiologists. RadioGraphics 36:554-572, 2016
28. Shinagare AB, Krajewski KM, Braschi-Amirfarzan M, et al: Advanced renal cell carcinoma: Role of the radiologist in the era of precision medicine. Radiology 284(2), 2017
29. Coppin C, Kollmannsberger C, Le L, et al: Targeted therapy for advanced renal cell cancer (RCC): A Cochrane systematic review of published randomized trials. BJU Int 108:1556-1563, 2011
30. Wahl RL, Jacene H, Kasamon Y, et al: From RECIST to PERCIST: Evolving considerations for PET response criteria in solid tumors. J Nucl Med 50(5 (Suppl)), 2009
31. Fletcher et al. WHO Classification of Tumors of Soft Tissue and Bone — 4th edition. ISBN 978-92-832-4491-2
32. Schuetze SM: Imaging and response in soft tissue sarcomas. Hematol Oncol Clin N Am 19:471-487, 2005
33. Messiou C, Collins DJ, Morgan VA, et al: Use of apparent diffusion coefficient as a response biomarker in bone: Effect of developing sclerosis on quantified values. Skeletal Radiol 43:205-208, 2014
34. Vilanova JC, Baleato-Gonzalez S, Romero MJ, et al: Assessment of musculoskeletal malignancies with functional MR imaging. Magn Reson Imaging Clin N Am 24:239-259, 2016
35. Soldatos T, Ahlawat S, Montgomery E, et al: Multiparametric MR imaging assessment of high-grade soft-tissue sarcomas. Radiology 278(3), 2016
36. VS Koshkin, V Bolejack, LH Schwartz, et al. Assessment of imaging modalities and response metrics in Ewing sarcoma: Correlation with survival. J Clin Oncol34:3680-3685.
37. Vallières M, Serban M, Benzyane I, et al: Investigating the role of functional imaging in the management of soft tissue sarcomas of the extremities. Phys Imaging Radiat Oncol 6:53-60, 2018
38. Drapé JL: Advances in magnetic resonance imaging of musculoskeletal tumors. Orthop Traumatol Surg Res 99S:S115-S123, 2013
39. Subhawong TK, Jacobs MA, Fayad LM: Diffusion-weighted MR imaging for characterizing musculoskeletal lesions. Radiographics 34:1163-1177, 2014
40. Khedr SA, Hassaan MA, Abdelrazek NM, et al: Diagnostic impact of echo-planar diffusion-weighted magnetic resonance imaging (DWI) in musculoskeletal neoplastic masses using apparent diffusion coefficient (ADC) mapping as a quantitative assessment tool. Egypt J Radiol Nucl Med 43:219-226, 2012
41. Yeom KW, Lober RM, Mobley BC, et al: Diffusion-weighted MRI: Distinction of skull base chordoma from chondrosarcoma. AJNR Am J Neuroradiol 34:1056-1061, 2013
42. Lall C, Bura V, Lee TK, et al: Diffusion-weighted imaging in hemorrhagic abdominal and pelvic lesions: Restricted diffusion can mimic malignancy. Abdom Radiol 43:1772-1784, 2018
43. Messiou C, Collins DJ, Morgan VA, et al: Optimising diffusion-weighted MRI for imaging metastatic and myeloma bone disease and assessing reproducibility. Eur Radiol 21:1713-1718, 2011
44. Giles SL, Messiou C, Collins DJ, et al: Whole-body diffusion-weighted MR imaging for assessment of treatment response in myeloma. Radiology 271(3), 2014
45. Ma X, Zhao X, Ouyang H, et al: Quantified ADC histogram analysis: A new method for differentiating mass-forming focal pancreatitis from pancreatic cancer. Acta Radiologica 55:785-792, 2014
46. Nakajo M, Fukukura Y, Hakamada H, et al: Whole-tumor apparent diffusion coefficient (ADC) histogram analysis to differentiate benign peripheral neurogenic tumors from soft tissue sarcomas. J Magn Reson Imaging 48:680-686, 2018
47. Umanodan T, Fukukura Y, Kumagae Y, et al: ADC histogram analysis for adrenal tumor histogram analysis of apparent diffusion coefficient in differentiating adrenal adenoma from pheochromocytoma. Magn Reson Imaging 45:1195-1203, 2017
48. Meng J, Zhu L, Zhu L, et al: Whole-lesion ADC histogram and texture analysis in predicting recurrence of cervical cancer treated with CCRT. Oncotarget 8:92442-92453, 2017
49. Poussaint TY, Vajapeyam S, Ricci KI, et al: Apparent diffusion coefficient histogram metrics correlate with survival in diffuse intrinsic pontine glioma: A report from the Pediatric Brain Tumor Consortium. Neuro-Oncology 18:725-734, 2016
50. Bharwani N, Miquel ME, Powles T, et al: Diffusion-weighted and multiphase contrast-enhanced MRI as surrogate markers of response to neoadjuvant sunitinib in metastatic renal cell carcinoma. Br J Cancer 110:616-624, 2014
51. Mabray MC, Cha S: Advanced MR imaging techniques in daily practice. Neuroimag Clin N Am 26:647-666, 2016

52. Yildirim A, Dogan S, Okur A, et al: The role of dynamic contrast-enhanced magnetic resonance imaging in differentiation of soft tissue masses. Eur J Gen Med 13:37-44, 2016
53. Dutoit JC, Vanderkerken MA, Verstraete KL: Value of whole-body MRI and dynamic contrast-enhanced MRI in the diagnosis, follow-up, and evaluation of disease activity and extent in multiple myeloma. Eur J Radiol 82:1444-1452, 2013
54. Spratt DE, Arevalo-Perez J, Leeman JE, et al: Early magnetic resonance imaging biomarkers to predict local control after high dose stereotactic body radiotherapy for patients with sarcoma spine metastases. Spine J 16:291-298, 2016
55. Napoli A, Anzidei M, Marincola BC, et al: MR imaging–guided focused ultrasound for treatment of bone metastasis. RadioGraphics 33:1555-1568, 2013